Ionization of dimethyluracil dimers leads to facile proton transfer in the absence of H-bonds

Amir Golan,[1,4] Ksenia B. Bravaya,[2] Romas Kudirka,[3] Oleg Kostko,[1] Stephen R. Leone,[1,4] Anna I. Krylov,[2] and Musahid Ahmed[1]

[1] Chemical Sciences Division, Lawrence Berkeley National Laboratory, Berkeley, CA 94720

[2] Department of Chemistry, University of Southern California, Los Angeles, CA 90089-0482

[3] Materials Sciences Division, Lawrence Berkeley National Laboratory, Berkeley California 94720

[4] Departments of Chemistry and Physics, University of California, Berkeley, CA 94720

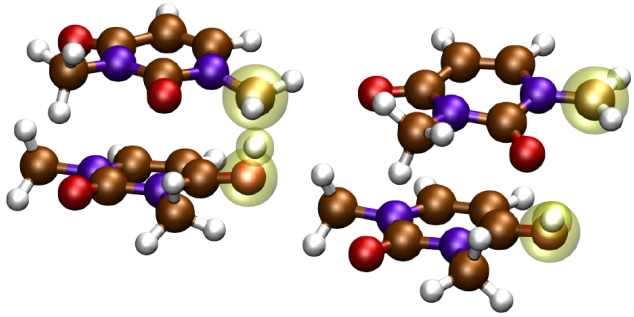

Efficient proton transfer (PT) across π-stacked pairs of methylated nucleic acid bases (NABs, 1,3-dimethyluracil) is observed upon ionization, even though methylation blocks the H-bonding sites and eliminates the H-bonded conformers in the neutral. Ionization driven PT in dimers of uracil and 1,3-dimethyluracil are investigated by tunable vacuum-ultraviolet (VUV) synchrotron mass spectrometry and electronic structure calculations. Ionization initiates efficient PT in H-bonded NAB pairs and the methylated species exhibit similar behavior with 85% of the ionized dimers dissociating with concurrent to a proton transfer. Deuterated dimethyluracil experiments reveal that PT occurs from the methyl groups and not from the aromatic CH sites. Calculations illuminate qualitative differences in the PT reaction coordinate in the π-stacked and H-bonded base pairs. PT in methylated dimers involves significant rearrangements of the two fragments facilitating a relatively low potential energy barrier of only 0.6 eV in the ionized dimer.

PT is ubiquitous in biological systems. Excited-state PT between nucleobases provides an efficient energy relaxation pathway(*1*) contributing towards intrinsic photostability of DNA. In oxidized DNA, PT separates the unpaired electron and positive charge between the two strands thus terminating the long-range hole migration(*2*). Excited-state PT is a key step in the photocycle of green fluorescent protein(*3*). PT across proteins and through membranes is one of the most important biochemical pathways in life(*4-5*). The mechanistic description of PT has always involved hydrogen-bonded networks particularly between Watson-Crick pairs induced by photoexcitation and/or photoionization of nucleobases(*6-7*). This report presents evidence and quantifies the PT in the absence of hydrogen bonds across π-stacked dimers of ionized nucleobases.

π-stacking, which is a common structural motif in biology, is prominent in DNA. It contributes to the structural integrity of the DNA double helix and plays an important role in radiation or ionization-induced processes(*8-10*) such as hole migration along the DNA strands(*5*), excimer formation, oxidized products, and fused dimer formation(*9-11*). Quantum mechanics explains the effects of π-stacking on electronically excited or ionized states in terms of efficient molecular orbital (MO) overlap that facilitates the delocalization of the excitation (or electron hole) over the stacked bases. However, the π-stacking arrangement is not efficient for PT. A crucial question is how does a proton find a transfer path in the absence of a guiding hydrogen-bonding network?

We investigate PT within a stacked pair of methylated uracil (U) bases, which represent a π-stacking motif in DNA. In 1,3-dimethyluracil (1,3-mU) dimer, a model system used in this work, methylation completely eliminates the H-bonded manifold in the neutral by blocking the usual H-bonding sites. In addition to interrogating electronic structure in model π-stacked systems, methylation of NABs has a broader significance. Methylation of DNA regulates gene expression, a basic mechanism in epigenetics(*12-13*) and a key reaction in DNA damage by certain carcinogenic agents. Methylation changes the ionization energies (IEs), redox potentials, and branching ratios between various ionization-induced processes and is crucial to understanding the electronic structure and function of DNA.

PT in NABs has been investigated in liquid(*14-15*) and gas phase dimers(*16-18*) and is identified as one of the relaxation pathways of ionized NAB dimers(*19-22*). These studies reveal that the photoionization relaxation patterns are different for π-stacked and H-bonded dimers. In the former, ionization may result in forming fused dimers with partially covalent bonding between the monomers and bonding energies of about 20 kcal/mol. In the latter, H-bonded dimers (AA, TT, AT, CC, GC), ionization leads to efficient PT. The resulting PT dimer ions are bound by 30-35 kcal/mol. Ground state PT between bases is endothermic (e.g., by 0.75 eV in AT), while in the ionized states it is

exothermic by 0.4-0.8 eV (see supplementary material (SM)). Hence, when sufficient energy is available to the ionized dimers, they dissociate producing protonated species.

Uracil is chosen since it has no tautomers to complicate the interpretation of the experimental results(*23*) and there is robust theory on ionization energetics of H-bonded and stacked pairs(*19-21*). This report shows that U dimers follow the behavior of other pyrimidine pairs forming protonated monomers upon ionization. The observed ionization appearance energies are supported by calculated IEs for H-bonded and π-stacked dimers. In contrast to the barrierless and one-dimensional reaction coordinate for PT in the U dimer, for 1,3-mU dimers our calculations show a 0.6 eV barrier and a complex reaction coordinate involving significant rearrangements of the two mU moieties for PT. The theoretical results support the experimentally observed large yield of protonated monomers upon ionization. To reveal the origin of the transferred proton, d6-1,3-dimethyuracil (d6-1,3-mU) is investigated, where only the two methyl moieties are deuterated, and the C-H moieties on the ring are not. This allows distinguishing whether the PT involves the methyl group or the uracil ring. The results show that deuterium transfer followed by dissociation of the dimer into the $(\text{d6-1,3-mUD})^+$ ion and the presumed deprotonated radical is the dominant reaction channel (up to 69% of the ionized dimers follow this channel while the other 31% remain as ionized dimers). This confirms that the transfer originates from the methyl group and not from the aromatic C-H sites. This observation of facile ionization induced PT reveals the importance of the previously neglected PT mechanisms in systems with no H-bonds, such as methylated NABs. In the context of mass spectrometry, this reaction can be described as an interesting case of so-called "chemical ionization", which has been observed in methane in the 60's and was used to softly ionize neutral species with a higher proton affinity(*24*). This ion-neutral reaction involving PT depends on the proton affinity of the reagents, and indeed Gronert et al.(*25*) measured the proton affinity of 1,3-mU in the gas phase to be 9.27 ± 0.13 eV and predicted that protonation takes place on the carbonyl groups. This high value offsets the energy penalty for breaking the CH bond in the ionized 1,3-mU(~ 9.4 eV), resulting in a relatively small (negative) reaction enthalpy for PT between the neutral and ionized monomers.

We employ tunable synchrotron radiation and a variety of ab initio approaches following protocols used in previous studies(*22, 26*) and described in detail in the SM. Briefly, the experiments are performed on a molecular beam apparatus coupled to a VUV monochromator on the Chemical Dynamics Beamline at the Advanced Light Source. A thermal vaporization source, effusive or a supersonic molecular beam (MB), are used to introduce the bases into the gas phase. The bases and their dimers are ionized by using photon energies between 8 eV and 11.5 eV and detected using reflectron mass spectrometry. Deuterated 1,3-mU was synthesized (see SM) since it is unavailable

commercially. Electronic structure calculations were performed using *Q-CHEM(27)* and employed methods ranging from EOM-IP-CCSD to DFT with range separated functionals and dispersion correction (wB97X-D).

A VUV-SPI mass spectrum of the U molecular beam features signals corresponding to U^+,U_2^+ and UH^+ and less than 3% of larger clusters (Figure 1A). The mass spectrum of 1,3-mU follows the same pattern (Fig. 1B). Figure 1C shows the photo-ionization efficiency (PIE) curves for the monomer, dimer, and protonated monomers for U and 1,3-mU generated by integrating the area of each mass spectral peak at different photon energies. The observed onsets of the PIE curves of U^+, U_2^+, 1,3-mU^+, and1,3-mU_2^+ correspond to the calculated adiabatic ionization energies (AIEs, see SM). In the uracil beam, the UH^+ channel exhibits a sharp rise at around 9.8 eV (Fig. 1C). Upon ionization of the methylated sample, the π-stacked dimer shows a significant signal for 1,3-mUH^+ (protonated 1,3-dimethyluracil ion) with an onset at ~9.35 eV demonstrating that PT is efficient in the methylated species despite the absence of H-bonds in the neutral.

We consider the following channels giving rise to the observed ion signals, where M is the investigated molecule (one monomer unit):

$$M + h\nu \rightarrow \quad M^+ \tag{1}$$

$$M_2 + h\nu \rightarrow \begin{cases} M_2^+ & (2) \\ MH^+ + (M-H)\cdot & (3) \\ M^+ + M & (4) \end{cases}$$

No other channels of dissociative ionization are detected in the mass spectra in agreement with previous studies(*28*). Larger clusters and microhydrated species due to traces of water present in the Ar carrier gas could potentially give rise to signal at the protonated monomer mass. However, these channels can be neglected for a number of reasons. In the case of d6-1,3-mU, no protonated monomers are observed; there is no notable signal for sample + water complex or higher uracil clusters; upon varying the backing pressure of the carrier gas, different amounts of dimers and trimers are detected in the supersonic MB while there is no concomitant change in the protonated monomer signal. The latter observation suggests that the presence of the trimers in the beam is negligible and that the beam is mainly monomers and dimers.

Furthermore, the effusive source signal shows no evidence of dimer or higher clusters and there is little change (less than 5%) in the PIE curve shape of the monomer signal U^+ (or 1,3-mU^+) compared to those formed in the molecular beam. This would suggest that dimer dissociation, channel (4), contributes less than 5% to the ion signal. With this in mind, only the first three channels, Eqns. (1)-

(3), need to be considered to explain the experimental results.

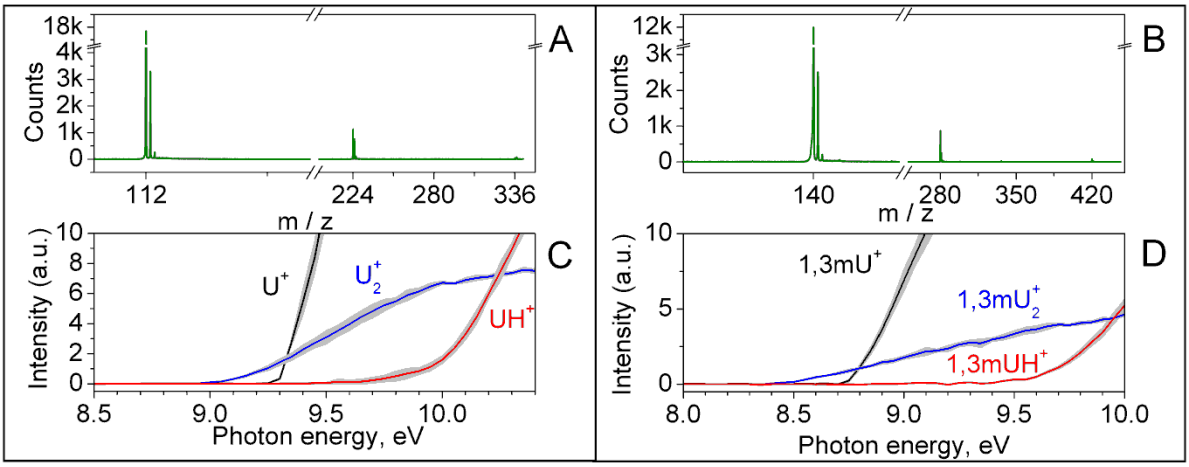

Fig. 1. Typical mass spectra and the PIE curves for U (A and C) and 1,3-mU (B and D) molecular beams. The signal at 112 corresponds to U^+, whereas the small peak at 113 is due to UH^+ in addition to 5.2% isotopic contribution. The peaks at m/z 140 and 141 correspond to 1,3-mU^+ and 1,3-mUH^+, respectively.

Energetics of channels (2) and (3) for the two representative systems(*19-20*), lowest-energy U_2 and 1,3-mU_2, are illustrated in Fig. 2. The diagram shows calculated adiabatic ionization energies (AIEs) that correspond to the PIE onsets of the respective species (provided that the Franck-Condon (FC) factors are favorable) and thermodynamic onsets corresponding to the dissociation channel leading to formation of the protonated monomer. The observed PIE onsets for the U^+ and 1,3-mU^+ agree within 0.1 eV with the respective computed AIEs (SM). The experimental onsets of the dimer PIE and protonated monomer appearance signals can also be compared to the AIEs and threshold energies (t) for formation of protonated monomers for the lowest energy dimers of U and 1,3-mU (t_{UH}^+ and $t_{1,3\text{-}mUH}^+$, respectively, in Fig. 2), with a caveat that the presence of other conformers in the MB may lead to discrepancies between the apparent onsets and those computed for the most stable species.

The most stable conformer of U_2 is a symmetric H-bonded structure (Fig. 2) bound by 0.70 eV (D_0). Higher in energy are several non-symmetric H-bonded structures followed by a π-stacked manifold that begins at around 0.4 eV above the lowest H-bonded conformer(*19, 29*) (the binding energy of the most stable π-stacked conformer is 0.33 eV (D_0)). The H-bond is rather conspicuous in the U dimer. The distance between the participating hydrogen and the oxygen of the complementary moiety is 1.76 Å, and the respective NH bond length changes by 0.02 Å relative to the monomer. Most importantly, the system is poised for PT owing to the nearly collinear arrangement of the three participating atoms (the value of the NHO angle is 177°).

Methylation eliminates the H-bonded manifold completely. The lowest-energy conformer of 1,3-mU_2 is a π-stacked one (Fig. 2.) and it is bound by 0.57 eV (D_0). These dimers provide a model for π-stacking interactions(*20*) in a native DNA structure, e.g., the equilibrium distance between the 1,3-mU in the gas phase dimer is 3.30 Å, to be compared with 3.33 Å separation between the bases in the DNA double helix. In addition to blocking the usual H-bonding interactions(*18, 29-30*), methylation increases the electron density in the π-system, which decreases the IEs and modulates the strength of π-stacking interactions(*20, 31-32*).

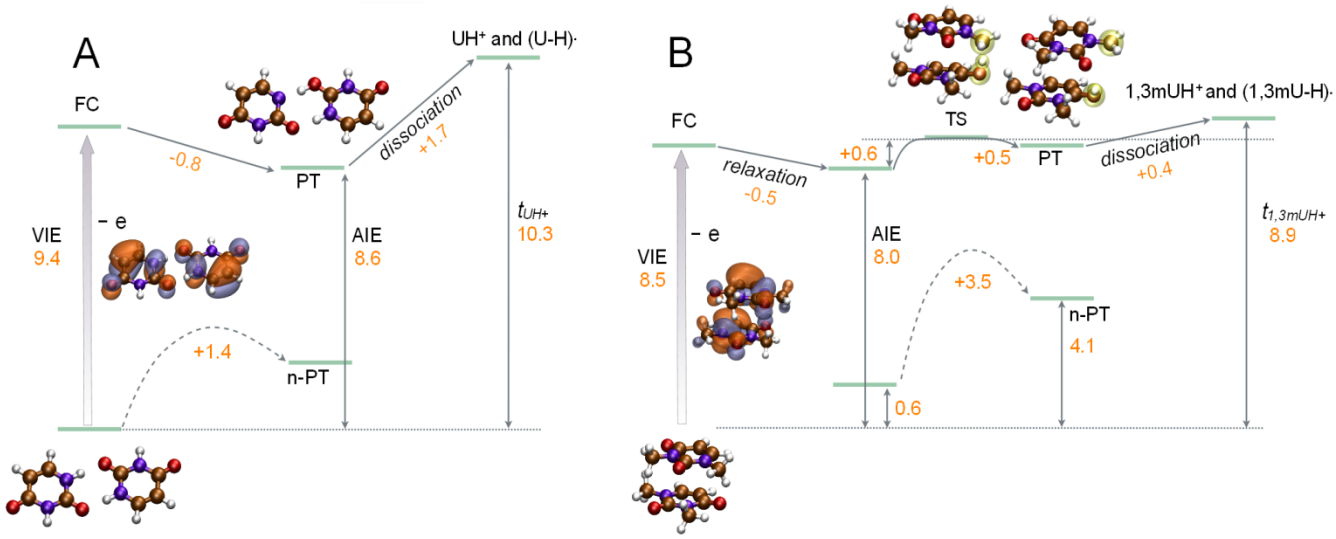

Fig. 2. Relevant computed energetics (eV) of the non-methylated H-bonded (A) and methylated uracil (B) dimers. The shape of the initial hole corresponding to the lowest ionized state is also shown (see molecular orbitals). Upon ionization, U_2^+ relaxes to the PT structure bound by 1.7 eV. In 1,3-mU_2^+, the FC relaxed structure, which resembles a fused dimer, (yellow spheres show the reaction moieties) is separated from the PT structure by a barrier (transition state (TS)). The dissociation energy of the PT structure is 0.4 eV. Threshold energies (*t*) for formation of protonated monomers for the lowest energy dimers of U and 1,3-mU are marked by t_{UH}^+ and $t_{1,3\text{-}mUH}^+$, respectively.n-PT refers to the PT structure in the neutral dimer. All energies except the vertical ionization energy (VIE) include zero point vibrational energy (ZPVE) correction.

Calculations predict that PT from methyl groups is more favorable energetically than PT from the aromatic ring. To verify this experimentally, we used deuterated 1,3-mU where CH_3 groups were replaced by CD_3 and the CH groups were left intact (d6-1,3-mU). Whereas the mass spectrum of 1,3-mU shows the monomer signal and a smaller protonated peak (Fig. 3 A), the d6-1,3-mU sample has three peaks, the first, corresponding to d6-1,3-mU^+ at mass to charge (m/z) 146, deuterium-transferred $(d6\text{-}1,3\text{-}mUD)^+$ at m/z 148, and a small peak at m/z 147. In figure 3B, trace (a). shows the ratio between protonated and unprotonated 1,3-mU signals; trace (b) shows the ratio between the deuterium-transferred and bare monomers (d6-1,3-mU+D/ d6-1,3-mU), which is almost identical to the analogous

1,3-mU curve shown in (a) The traces in (B) begin with a constant background (~0.072, and 0, respectively) due to the natural abundance of C_{13} and N_{15} isotopes. Then they rise sharply at ~9.6 eV with a small shallow slope beginning around 9.35 eV, indicating the onset for PT. The ratio between m/z 147 and 146 is photon-energy-independent, indicating that the m/z 147 peak arises from just the isotope contribution and not hydrogen transfer (Figure 3 B, trace (c)).

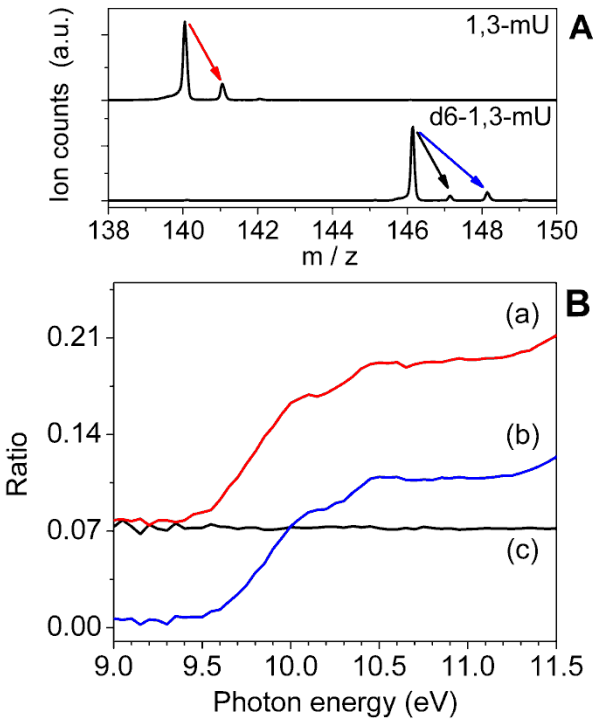

Fig. 3. Mass spectra obtained at 10.50 eV for 1,3-mU and d6-1,3-mU zoomed in to show the monomer and protonated / deuterated peaks (A). The arrows refer to ratios between several peaks as shown in panel B. The ratio between the 1,3-mU^+ signal and $(1,3\text{-}mUH)^+$ (m/z 140 divided by m/z 141) is shown in trace (a). Following the natural isotope background of 0.072% arising from the 0.0107% and 0.368% contributions of C_{13} and N_{15}, respectively, is the PT onset at 9.35 eV. Traces (b) and (c) show the ratio between the monomer signal at m/z 146 and the peaks at m/z 148 and 147, respectively. Trace (b) exhibits the same energy dependence as trace (a), while trace (c) remains constant demonstrating no (observable) hydrogen is transferred from the C-H groups on the aromatic ring.

To establish the relationship between the apparent onsets for PT and the underlying mechanism, we consider the energetics of the ionization-induced intramolecular PT in NAB dimers, the first step leading to formation of the protonated monomers. In U_2, PT is exothermic and barrierless in the ionized state. Methylation results in a significant barrier (0.6 eV) for PT in ionized 1,3-mU_2. The structure after PT is 0.5 eV higher in energy than the relaxed non-PT structure and is isoenergetic in the vertical FC geometry. The thermodynamic onsets for formation of protonated monomers are

computed as the energy difference between the initial neutral dimer and the products, UH^+ and $(U–H)\cdot$ (or 1,3-mUH^+ and $(1,3\text{-}mU–H)\cdot$). For the lowest energy dimers of U_2 and 1,3-mU_2, the PT channel opens at 10.25 eV and 8.93 eV, respectively. Note that the shift in the thermodynamic onset for the d6-1,3-mUD^+ due to the difference in zero point vibrational energy (ZPVE) is only 0.02 eV and the resulting threshold energy is 8.95 eV. Importantly, for both UH^+ and 1,3-mUH^+ systems, the thermodynamic onsets should correspond to the appearance curve onsets because there is no barrier for proton transfer in ionized H-bonded U_2 and the transition state (TS) energy is below the thermodynamic onset in the 1,3-mU_2. If higher-energy conformers are present in the beam, the apparent onsets will be lowered. The binding energy of the lowest energy dimer conformer (D_0=0.57 eV) also defines the uppermost energetically possible 1,3-mU_2 dimer. Hence, the most conservative estimate of the lower bound of the PT channel onset for 1,3-mU_2 is 8.36 eV. This requires population of conformers that are 0.57 eV above the lowest one, rather unlikely even assuming non-Boltzmann distributions in the thermal desorption sources used. A similar estimate provides 9.10 eV as the lower bound energy for the PT channel onset for U_2. Therefore, theory predicts that PT channels should be available above 9.10 eV and 8.36 eV for U and 1,3-mU, respectively, and that the signal from the lowest energy dimer starts to contribute at 10.25 eV and 8.93 eV, respectively. Indeed, the observed experimental onsets for UH^+ and 1,3-mUH^+ signals lie above the predicted lower bound of the PT channel onsets, possibly due to unfavorable FCFs and population of higher energy conformers of the dimers in the MB. For UH^+, the sharp rise of the signal at 9.8 eV is in excellent agreement the values predicted for two higher energy H-bonded dimers of U_2 (see SM). In summary, the observed onsets of the appearance of protonated U and 1,3-mU are within the theoretically predicted bounds, and the sharp UH^+ signal rise correlates with the theoretical values of the most abundant conformers.

To obtain detailed information of the PT channel, we analyzed the branching ratios between the PT and formation of the ionized dimer. The contribution of the dimer dissociation to the monomer signal, channel (4), is not substantial, and therefore ionized dimers give rise to only U_2^+ or UH^+ signals (1,3-mU_2^+ and 1,3-mUH^+ in the methylated species).

Consequently, the branching ratio for the PT channel is given by:

$$\frac{MH^+}{M_2^+ + MH^+} \tag{5}$$

where MH^+ and M_2^+ are the PIE signals of the protonated monomer and the dimer, respectively. These ratios for U, 1,3-mU, and d6-1,3-mU are shown in Fig. 4. These ratios characterize the efficiency of the PT channels in different species.

Asymptotically, the efficiency of PT in uracil and dimethyluracil is remarkably similar and approaches 85% fraction of the ionized dimers for U and 1,3-mU. The deuterated curve lags behind the non-deuterated signal and approaches a lower asymptotic value of 69% (while the other 31% do not fragment and remain as ionized dimers). Similar values derived from an RRKM model are in semi-quantitative agreement with the experiment results, 75 % and 67 % for 1,3-mUH$^+$ and d6-1,3-mUD$^+$, respectively (see SM). The small effect of H/D substitution on the observed yield of protonated monomers points to the complex reaction coordinate for the PT process. The presence of different conformers in the molecular beam, possible involvement of multiple ionized states with different ionization cross-sections, potential energy surfaces, and anharmonic effects make quantitative predictions of kinetic isotope effects extremely difficult in these systems.

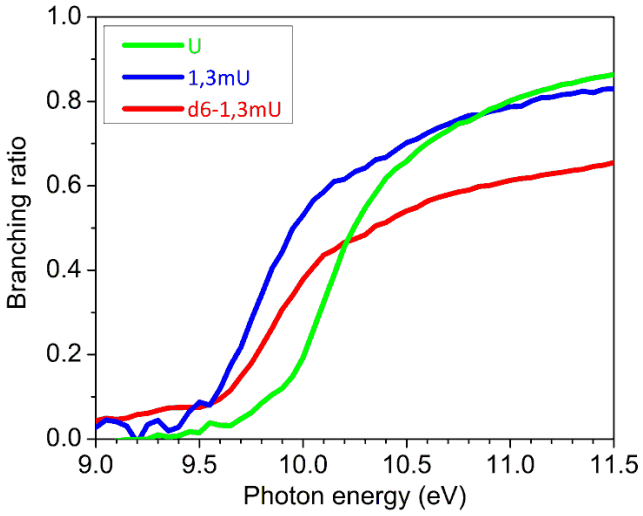

Fig. 4. Experimental branching ratios for the PT channel in the U, 1,3mU, and d6-1,3-mU beams. While showing different onsets, the PT efficiency in uracil and dimethyluracil is remarkably similar and reaches 85%. The deuterated curve lags behind the non-deuterated signal and approaches a lower asymptotic value of 69%.

The nature of motions promoting low-energy PT in the ionized state is very different for H-bonded and π-stacked systems. In the former case, the PT reaction coordinate corresponds to a simple proton motion between the two U moieties owing to an almost linear H-bond (∠(N-H-O)=177º) and a relatively short distance between the proton-accepting and proton-donating atoms (2.794 Å at the FC geometry). Due to the collinear arrangement, the elongation of one of the bonds (N-H) implies shortening of the other (O-H) bond, and no large changes are observed in other degrees of freedom (e.g., relative orientation of the fragments) along the PT reaction coordinate. Thus, PT is essentially a

one-dimensional process in these H-bonded systems.

In contrast, the structure of the stacked 1,3-mU_2 dimer is not optimal for PT, i.e., the C-O separation is 3.136 Å and $\angle$(C-H-O) = 107º at the FC-relaxed geometry. Therefore, a considerable rearrangement of the bases along the PT pathway is required to make the process energetically accessible.

This is illustrated by the two-dimensional potential energy surface (PES) scan and the PT reaction coordinate shown in Fig. 5(A). Although one can imagine multiple reaction pathways on this excited PES, the lowest energy PT path involves the concerted change in the distances between the proton and the donating (C-H) and accepting (O-H) atoms. The TS is nearly symmetric with respect to the C-H and O-H separation. Contrary to the H-bonded conformer, a simple elongation of the C-H bond does not correlate with the O-H bond contraction, which requires reorientation of the bases. Thus, one-dimensional PES scans along either the C-H or O-H bonds (with all other degrees of freedom relaxed) results in a much higher PT barrier. The complex character of the PT reaction coordinate is illustrated by the changes in C-O separation and the distance between centers of mass of the bases along the points corresponding to the minimal energy path on the 2D surface (Fig. 5(B)). The C-O distance decreases by 0.6 Å as the system moves from the FC-relaxed structure to the TS. The shallow (with respect to inter-fragment relative motion) shape of the PES determined by weak electrostatic and dispersion interactions in the ion allows for significant reorientation of the bases along the PT coordinate necessary to achieve a favorable alignment of the C-H-O moiety. Near the TS, the dimer assumes a T-shaped structure manifested by a large increase in the center of mass (COM) separation shown in Fig. 5(C). As the system passes over the TS, it relaxes back to a stacked geometry.

Such a complex reaction coordinate may have implications for the ionization-induced PT between methylated stacked bases in a native environment where their relative motion is constrained. The backbone can make the TS structure inaccessible, thereby reducing the efficiency of PT between the stacked bases in real DNA. The effects of thermal structural fluctuations, therefore, can be of crucial importance for ionization-induced PT in DNA, which deserves further theoretical and experimental studies.

The evolution of the electronic wave function along the PT reaction coordinate is demonstrated by the shapes of MOs (Fig. 5(D)) at the initial equilibrium (MIN), the final (PT), and the TS structures. The initial hole is delocalized over both fragments, whereas in the TS and PT structures the unpaired electron is localized on the proton-donating base. Note that the shape of the MO in the PT and TS structures reveals hole delocalization over the C-H sigma bonds. Therefore, the change in the electronic state character along the reaction path facilitates PT by reducing C-H bonding character and

weakening the C-H bonds.

Whereas the complexity of the system does not allow establishing all possible PT pathways and quantitative prediction of the PT rates, the experimental results unambiguously demonstrate that the PT channel is very efficient in methylated species and that the reaction begins near the thermodynamic onset. By considering this as a model system of stacked base pairs, it is demonstrated that ionization-induced PT encounters only a moderate energy barrier (0.6 eV or 14 kcal/mol) owing to the concerted reaction coordinate and complex evolution of the electronic wave function. These findings imply that protons may efficiently transfer along the stacked ionized systems in the absence of H-bonds in the neutral and that methylation of DNA would not prevent excited/ionized-state PT, which is important in photoexcitation and oxidation induced processes.

It is possible that similar PT mechanisms could be operational in other stacked systems prevalent in biology. For instance, plant biomass is made up of an intricate array of inter and intra-molecular hydrogen-bonded networks, and within this arrangement there are stacked π-systems where such PT mechanisms could be operational upon photoexcitation and ionization.

These results pave the way for more sophisticated experiments to directly probe the nature and dynamics of PT in stacked systems. Ultrafast experiments using VUV photons should allow direct mapping of PT rates, while two-color infrared-VUV spectroscopy should provide structural insight into the PT mechanism. Inclusion of time-resolved pump-probe spectroscopy would allow molecular movies of PT to be generated. This will provide unique understanding of these quantum mechanical processes prevalent in biological systems.

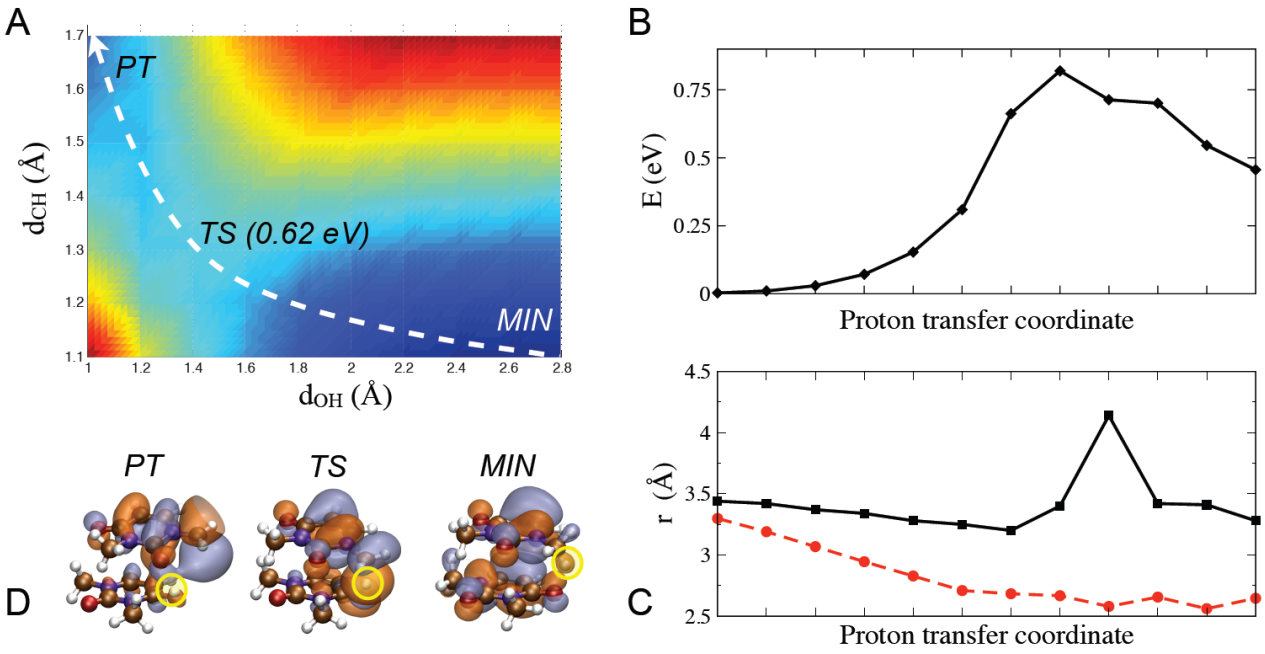

Fig. 5. The 2D PES scan (A) show the complex PT path in the dimer ion, 1,3-mU_2^+ involving the concerted change in the distances between the proton and the donating (C-H) and accepting (O-H) atoms. The energy along the PT reaction coordinate is shown in panel B (note that the barrier height is higher than in panel A since it does not include ZPVE). Panel C illustrates the change in the C-O distance and the distance between centers of mass (COM) of the monomers along the PT reaction minimum energy path on the computed 2D PES demonstrating the significant reorientation of the bases necessary to achieve a favorable alignment of the C-H-O moiety. The MOs at the initial (MIN), final (PT), and TS structures of the lowest-energy 1,3-mU_2^+ conformer with a green circle marking the transferred proton demonstrate the evolution of the wave function along the PT pathway (D). Energies were computed with ωB97X-D/6-31+G(d,p) and include ZPVE correction.

Acknowledgment

The experiments were carried out at the Advanced Light Source and the d6-1,3-mU was synthesized at the Molecular Foundry both at Lawrence Berkeley National Laboratory; Berkeley participants are supported by the Office of Science, Office of Basic Energy Sciences, of the US Department of Energy under Contract No. DE-AC02-05CH11231, through the Chemical Sciences Division (A.G., O.K., S.R.L., M.A.) and the Materials Sciences Division (R.K.). R.K. is also supported by the Defense Threat Reduction Agency (IACRO-B0845281). This work was conducted in the framework of the *iOpenShell* Center for Computational Studies of Electronic Structure and Spectroscopy of Open-Shell and Electronically Excited Species (iopenshell.usc.edu) supported by the National Science Foundation through the CRIF:CRF CHE-0625419+0624602+0625237 and CHE-0951634 (A.I.K.) grants.

References

1. T. Schultz *et al.*, *Science* **306**, 1765 (2004).
2. A. K. Ghosh, G. B. Schuster, *J. Am. Chem. Soc.* **128**, 4172 (2006).
3. J. T. M. Kennis *et al.*, *Proc. Nat. Ac. Sc.* **101**, 17988 (2004).
4. P. Mitchell, *Nature* **191**, 144 (1961).
5. T. Chakraborty, *Charge Migration in DNA: Perspectives from Physics, Chemistry, and Biology*, (2007).
6. A. L. Sobolewski, W. Domcke, C. Hättig, *Proc. Nat. Ac. Sc.* **102**, 17903 (2005).
7. S. Perun, A. L. Sobolewski, W. Domcke, *J. Phys. Chem. A* **110**, 9031 (2006).
8. C. E. Crespo-Hernandez, B. Cohen, P. M. Hare, B. Kohler, *Chem.l Rev.* **104**, 1977 (2004).
9. C. T. Middleton *et al.*, *Ann. Rev. Phy. Chem.* **60**, 217 (2009).

10. S. Kanvah *et al.*, *Acc. Chem. Res.* **43**, 280 (2009).
11. W. J. Schreier *et al.*, *Science* **315**, 625 (2007).
12. A. Portela, M. Esteller, *Nat. Biotech.* **28**, 1057 (2010).
13. B. Youngblood, C. W. Davis, R. Ahmed, *Int.l Immun.* **22**, 797 (2010).
14. K. Kobayashi, S. Tagawa, *J. Am. Chem. Soc.* **125**, 10213 (2003).
15. A. Adhikary, D. Khanduri, M. D. Sevilla, *J. Am. Chem.Soc.***131**, 8614 (2009).
16. N. Gador *et al.*, *J. Phys. Chem. A* **111**, 11743 (2007).
17. E. Nir, C. Plutzer, K. Kleinermanns, M. de Vries, *Eur. Phys. J. D* **20**, 317 (2002).
18. C. Plutzer, I. Hunig, K. Kleinermanns, *Phys. Chem. Chem. Phys.* **5**, 1158 (2003).
19. A. A. Zadorozhnaya, A. I. Krylov, *J. Chem. Theo. Comp.* **6**, 705 (2010).
20. A. A. Zadorozhnaya, A. I. Krylov, *J. Phys. Chem. A* **114**, 2001 (2010).
21. A. A. Golubeva, A. I. Krylov, *Phys. Chem. Chem. Phys.* **11**, 1303 (2009).
22. K. B. Bravaya, O. Kostko, M. Ahmed, A. I. Krylov, *Phys. Chem. Chem.Phys.* **12**, 2292 (2010).
23. M. S. de Vries, P. Hobza, *Ann. Rev. Phys. Chem.* **58**, 585 (2007).
24. M. S. B. Munson, F. H. Field, *J. Am. Chem.Soc.* **88**, 2621 (1966).
25. S. Gronert, W. Y. Feng, F. Chew, W. Wu, *Int. J. Mass Spec.* **195-196**, 251 (2000).
26. L. Belau, K. R. Wilson, S. R. Leone, M. Ahmed, *J. Phys. Chem. A* **111**, 7562 (2007).
27. P. K. Sahu, R. K. Mishra, S.-L. Lee, *J. Phys. Chem. A* **109**, 2887 (2005).
28. H. W. Jochims, M. Schwell, H. Baumgartel, S. Leach, *Chem. Phys.* **314**, 263 (2005).
29. M. Kabelac, P. Hobza, *Chem. Eur. J.* **7**, 2067 (2001).
30. M. Kabelac, P. Hobza, *J. Phys.l Chem. B* **105**, 5804 (2001).
31. Y. G. He, C. Y. Wu, W. Kong, *J. Phys. Chem. A* **108**, 943 (2004).
32. H. Satzger, D. Townsend, A. Stolow, *Chem. Phys. Let.* **430**, 144 (2006).